Young's Double-Slit Experiment with Atoms: A Simple Atom Interferometer

O. Carnal and J. Mlynek

Fakultät für Physik, Universität Konstanz, D-7750 Konstanz, Germany

(Received 4 March 1991)

An atomic interferometer based on a Young's-type double-slit arrangement has been demonstrated. A supersonic beam of metastable helium atoms passes through a 2-μm-wide slit in a thin gold foil. This transversely coherent beam impinges on a second microfabricated transmission structure, consisting of two 1-μm-wide slits at a lateral distance of 8 μm. This double slit defines two possible paths on which the atoms can reach the detector slit. The good visibility of the observed fringes should make it possible to measure differential phase shifts in the interferometer of $\frac{1}{3}$ rad in less than 10 min.

Matter-wave interferometry is a well established field in physics. Interferometers with de Broglie waves have been demonstrated for electrons and neutrons and extensively used for fundamental tests of quantum-mechanical predictions.[1] The construction of an interferometer for *atoms* is rendered difficult by the fact that atoms carry no charge like electrons and cannot penetrate through condensed matter like neutrons. Therefore novel techniques are required to provide coherent beam splitters for atomic waves. In the last few years, different proposals were published on how to realize an atomic interferometer.[2] In this Letter, we present probably the simplest configuration in which the atoms cover two spatially well separated paths: the quantum-mechanical analog to Young's double-slit interferometer in classical optics (see Fig. 1), which has already been demonstrated for electrons[3] and neutrons.[4] In our arrangement, the slits are mechanical transmission structures with widths in the micrometer range. As atomic species we used metastable helium atoms: The helium atom has a low mass which leads to a large de Broglie wavelength. Moreover, helium is inert, thus facilitating the use of very delicate transmission structures,[5] and the production of an intense helium beam is a well-known technique. In addition, metastable helium atoms are easily detected and have optical transitions in the near infrared, so that their internal and external degrees of freedom can be manipulated by laser fields.

The scheme of our experimental setup is shown in Fig. 2; details of the apparatus are given elsewhere.[5] An intense atomic beam of helium atoms is produced by a supersonic gas expansion. A collinear electron-impact excitation creates metastable atoms in the states 2^1S_0 and 2^3S_1, with relative populations of 90% and 10%, respectively.[6] After the excitation, the beam of metastable atoms has a spectral brightness of $B \cong 10^{17}$ (metastable atoms)/(sec sr cm^2) (Ref. 7) and a velocity ratio of $v_0/\Delta v \cong 15$–20, where v_0 denotes the mean velocity in the beam and Δv the full width at half maximum of the Gaussian velocity distribution. The mean velocity of the atoms, and therefore the mean de Broglie wavelength,
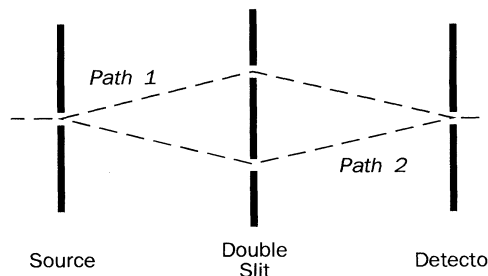

FIG. 1. Scheme of a double-slit interferometer. The atoms can move along two spatially separated paths from the source to the detector.
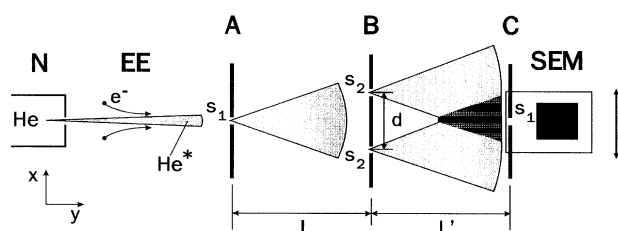
FIG. 2. Schematic representation of the experimental setup: nozzle system and gas reservoir N; electron impact excitation EE; entrance slit A, double slit B, and detector screen C; secondary electron multiplier SEM (mounted together with C on a translation stage). Dimensions: $d = 8$ μm, $L = L' = 64$ cm; slit widths: $s_1 = 2$ μm, $s_2 = 1$ μm.
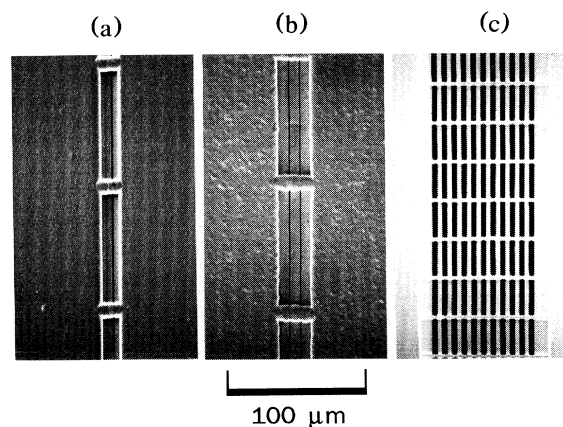

100 μm

FIG. 3. Scanning-electron-microscope pictures of the microfabricated transmission structures, with the slit structures in the vertical direction and the support gratings in the horizontal direction: (a) entrance and detection slit (slit width $s_1 = 2$ μm); (b) double slit (slit width $s_2 = 1$ μm and slit separation $d = 8$ μm); (c) detection grating (grating periodicity 8 μm). The 100-μm scale is the same for all three pictures.

can be adjusted by changing the temperature of the gas reservoir and the nozzle system. At present, the reservoir temperature can be set to $T = 295$ K, corresponding to a mean de Broglie wavelength of $\lambda_{dB} = 0.56$ Å, or to $T = 83$ K, corresponding to $\lambda_{dB} = 1.03$ Å.

After the electron-impact excitation, the atoms pass through a slit with a width of $s_1 = 2$ μm, imprinted in a thin gold foil. A scanning-electron-microscope picture of this transmission structure is shown in Fig. 3(a). The total slit height amounts to 4 mm. After having traveled $L = 64$ cm downstream, the atoms pass through two 1-μm-wide slits, separated by 8 μm. This double slit is irradiated coherently, as the atomic waves passing the narrow entrance slit are, in analogy to classical optics, transversely coherent over an angle $\theta = \lambda_{dB}/s_1 \equiv 5 \times 10^{-5}$ rad. This double-slit structure [see Fig. 3(b)] is 2 mm high. The edges forming both the entrance and the double slit are 1 μm thick, whereas the surrounding gold foil is 20 μm thick. An additional support grid, having a periodicity of 100 μm and made of 11-μm-wide by 20-μm-thick gold bars, ensures that the edges of each slit are parallel to better than 10^{-4} rad. This support structure reduces the total transmission of the slits by approximately 10%. The atomic waves emerging from the double slit then recombine coherently and produce an interference picture in the atomic density distribution. This density profile is detected in a plane located another $L' = 64$ cm behind the double slit. The interference pattern can be monitored either with a 2 μm slit, identical to the entrance slit, or with a grating with a periodicity of 8 μm formed by ten bars [see Fig. 3(c)]. The complete detector system consists of a secondary electron multiplier (SEM) behind a single gold foil with imprinted microfabricated slit and grating, both (SEM and foil) mounted on the same translation stage. The detector system can be moved in steps of 1.88 μm by means of a stepper motor and a precise lead screw. The electronic pulses generated by the SEM are preamplified, discriminated against background noise, and finally added up by a counter. The resulting background noise level of the

detector without atomic beam amounted to only 2–3 counts/min. The great number of atoms remaining in the ground state (approximately 10^6 times more than in the two metastable states) does not have any effect on the experiments, since ground-state atoms are not detected. The three successive microfabricated slit structures forming the interferometer were adjusted parallel to better than 5×10^{-4} rad using the diffraction pattern of a 5-mW HeNe laser: For this purpose, the laser beam passed through 20-μm-wide adjustment slits, which are imprinted in the same three gold foils as the transmission structures.

The microfabricated transmission structures were manufactured by Heidenhain Inc., using the manufacturing process "DIAGRID."[8] In this special process, a flat glass substrate is covered with an electrode layer. A thin film of insulating photoresist, put on top of this electrode layer, is structured by a printing process in absolute contact with the original chrome mask. A thin gold film is then deposited by galvanoplating on the photoresist depth profile. No gold accumulates where photoresist is still present. After peeling the gold layer off the substrate, one obtains a gold foil with transmission structures. These thin gold films are finally mounted on flat stainless-steel holders. The gold structures manufactured with this photolithographic technique have extremely precise and steep edges, as shown in Figs. 3(a)–3(c).

The interference pattern, obtained with our double-slit setup, can be calculated to good approximation in the Fraunhofer limit. In the detection plane, we expect a modulated intensity distribution with a periodicity $dx = L'\lambda_{dB}/d$ and an envelope with a full width of $2L'\lambda_{dB}/s_2$;

here d and s_2 are the distance between the two slits and the width of the double slits, respectively. The total number of interference maxima is further reduced by the finite velocity ratio. In a first experiment, we investigated the interference pattern with the single 2-μm slit by moving it laterally to the beam axis in 1.88-μm steps. The integration time at each detector position was 10 min, in order to obtain a reasonable signal-to-noise ratio. The experimental results for two different atomic wavelengths are shown in Figs. 4(a) and 4(b). With a de Broglie wavelength of $\lambda_{dB} = 0.56$ Å, the average distance between two maxima is $dx = 4.5 \pm 0.6$ μm [Fig. 4(a)], which agrees well with the theoretical value $dx = L'\lambda_{dB}/d = 4.5$ μm. The different interference maxima are not resolved completely, since the interference period is only twice the detector slit width. The scan covers half of the interference pattern, fading out on the right side, due to the finite width of the two slits and the residual velocity spread in the beam. In order to improve the visibility of the fringes we repeated the same experiment, but with a nozzle temperature of $T = 83$ K ($\lambda_{dB} = 1.03$ Å). In this case, the distance between two maxima increased and was measured to be 8.4 ± 0.8 μm which is close to the theoretical value of 8.2 μm. In Fig. 4(b) we find a visibility V (Ref. 9) of the fringes greater than 60%, if we subtract the detector background. The difference from the expected value of $V = 80\%$ could be due to a small
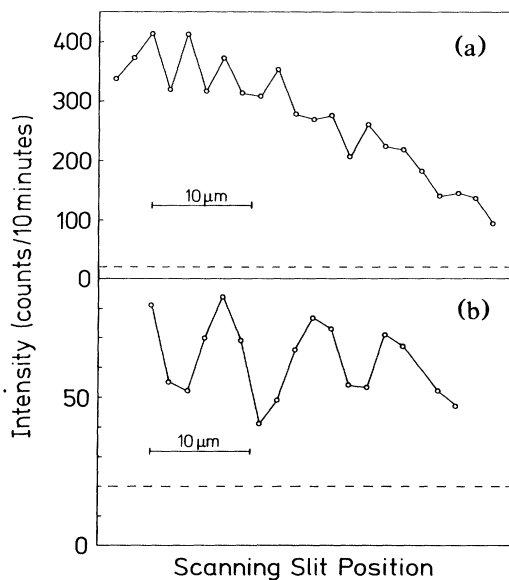
misalignment of the three transmission structures or to small-angle collisions of the atoms with the background gas in the vacuum chamber (background pressure $p \cong 5 \times 10^{-7}$ mbar). Since these incoherent processes destroy the phase information between the two paths, this would cause a broad unstructured background signal. Because of the long integration times and a slow thermal drift inside the beam machine, it was not possible with the actual beam intensity to monitor the whole interference pattern in one scan. Nevertheless, the scans displayed in Fig. 4 cover a sufficiently large part of the atomic density distribution, so that the presence of an interference pattern is clearly demonstrated.

Instead of using a single slit, a grating can be inserted to monitor the intensity distribution. If the grating period and the period of atomic interference pattern coincide, the signal at the detector is maximum when the slits are at positions of the intensity maxima, and a minimum signal occurs when the grating is displaced by half a grating period. Scanning the interference structure with the grating yields an interference picture similar to the one obtained with a single slit in the detector plane [Fig. 4(b)], but with a much higher count rate. For our experimental geometry, the grating period of 8 μm was chosen so that it matched the period of the interference pattern at $L' = 64$ cm for $\lambda_{dB} = 1.03$ Å. The slits are approximately 4 μm wide, resulting in a grating transmission of 50%. Monitoring the interference pattern with the grating is of interest for applications of this interferometer where only the relative phase between the two different paths and not the actual shape of the interference pattern is important. Figure 5 shows a typical result of an experimental run with the 8-μm grating in the detector plane and a wavelength of $\lambda_{dB} = 1.03$ Å. The average distance between two maxima is determined to be 7.7 ± 0.5 μm, which differs from the theoretical value by about 5% and is within the limited accuracy of

FIG. 4. Measured atomic intensity profiles in the detector plane as a function of the lateral detector position x. The profile is probed with the 2-μm-wide single slit. Atomic wavelength (a) $\lambda_{dB} = 0.56$ Å and (b) $\lambda_{dB} = 1.03$ Å. The number of detected atoms during 10 min is plotted on the vertical axis. The dashed line is the detector background, with the atomic beam blocked in front of the entrance slit. The line connecting the experimental data is a guide to the eye.
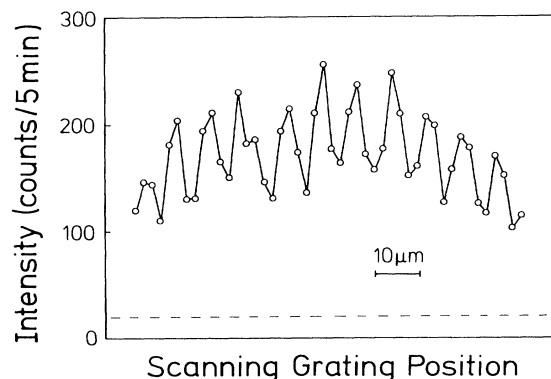

FIG. 5. Atomic density profile, monitored with the 8-μm grating in the detector plane, as a function of the lateral grating displacement. The dashed line is the detector background. The line connecting the experimental points is a guide to the eye.

out setup. The visibility amounts to 30%, whereas 50% can be expected under ideal conditions. The total number of detected atoms is increased by a factor of 10 compared to the case where the interference pattern is monitored with the single slit. With this increase in signal, the integration time could be lowered to 5 min/point, thus reducing the effect of thermal drifts. Since the number n of detected atoms in a given time interval is distributed around a mean number $\bar{n}$ according to Poissonian statistics, the mean relative error at each detector position is given by $1/\bar{n}^{1/2}$. In our case the mean relative error is less than 10% at any detector position; measurements of phase shifts on the order of $\frac{1}{3}$ rad are therefore possible within 10 min.

To improve the signal-to-noise ratio for future experiments, the brightness of the beam has to be increased. Recent experiments have shown that transverse laser cooling of a metastable helium beam can increase the beam intensity by more than a factor of 10.[10] Since a double-slit interferometer is sensitive to a velocity spread in the atomic beam, a very narrow velocity distribution is a prerequisite for precision measurements. Additionally, a larger separation of the double slit is only efficient in connection with an increased velocity ratio. In this respect, investigations by our group on a beam of metastable argon atoms have demonstrated that longitudinal laser cooling in the center-of-mass frame of the atoms can increase the speed ratio in the beam to $v_0/\Delta v > 500$.[11] Thus with present laser cooling techniques, it should be possible to increase the spectral brightness of the He* beam by at least 2 orders of magnitude.

An interferometer of the double-slit type has several applications. Since both paths are spatially separated, it is possible to introduce a relative phase shift between the two arms of the interferometer by applying an external potential to the atoms that varies over the distance between the two paths. Many experiments already carried out with neutrons can be translated to atoms, like tests of the Aharonov-Casher effect, demonstrations of Berry's phase, or measurements of phase changes caused by a rotating or accelerated reference frame.[1] In all these cases, atom interferometry benefits from the larger mass and magnetic moment of atoms compared to neutrons.

Moreover, atom interferometers offer the possibility to investigate various effects due to resonant light-atom interactions. The influence of spontaneous decays on the phase information can be tested, e.g., by irradiating one or both paths with resonant laser light.[12] Another interesting situation arises if an off-resonant laser beam of high intensity induces a pseudopotential for the motion of the atomic center of mass; under appropriate experimental conditions, spontaneous decay processes can then be neglected.

In conclusion, the atomic interferometer presented in this paper is of great simplicity, since all splitting and recombining elements are mechanical structures. Moreover, helium atoms combine many properties that are of great importance when building an interferometer, for example, their low mass and high detection efficiency in the metastable state. First experiments to study laser-induced phase shifts are now in preparation in our laboratory.

[1]See, e.g., *Proceedings of the International Workshop on Matter Wave Interferometry, Vienna, 1987,* edited by G. Badurek, H. Rauch, and A. Zeilinger [Physica (Amsterdam) **151B** (1988)].

[2]See, e.g., V. P. Chebotayev, B. Ya. Dubetsky, A. P. Kasantsev, and V. P. Yakovlev, J. Opt. Soc. Am. B **2**, 1791 (1985); P. J. Martin, B. G. Oldaker, A. H. Miklich, and D. E. Pritchard, Phys. Rev. Lett. **60**, 515 (1988); D. W. Keith, M. L. Schattenburg, H. I. Smith, and D. E. Pritchard, Phys. Rev. Lett. **61**, 1580 (1988); J. F. Clauser, Physica (Amsterdam) **151B**, 262 (1988); J. Schwinger, M. O. Scully, and B.-G. Englert, Z. Phys. D **10**, 135 (1988); Ch. J. Bordé, Phys. Lett. A **140**, 10 (1989).

[3]C. Jönsson, Z. Phys. **161**, 454 (1961).

[4]A. Zeilinger, R. Gähler, C. G. Shull, W. Treimer, and W. Mampe, Rev. Mod. Phys. **60**, 1067 (1988).

[5]O. Carnal, A. Faulstich, and J. Mlynek (to be published); A. Faulstich, O. Carnal, and J. Mlynek, in Proceedings of the International Workshop on Light Induced Kinetic Effects on Atoms, Ions and Molecules, Elba, Italy, 1990, edited by L. Moi *et al.* (to be published).

[6]W. Sesselmann, B. Woratschek, J. Küppers, G. Ertl, and H. Haberland, Phys. Rev. B **35**, 1547 (1987).

[7]The spectral brightness B is defined as (particles sr^{-1} $time^{-1} area^{-1}$) $v/\Delta v$.

[8]The manufacturing process "DIAGRID" is a trademark of Heidenhain Inc. (Traunreut, Germany).

[9]V is defined by $V = (I_{max} - I_{min})/(I_{max} + I_{min})$, where I_{max} and I_{min} denote the maximum and minimum intensities of the interference pattern.

[10]A. Aspect, N. Vansteenkiste, R. Kaiser, H. Haberland, and M. Karrais, Chem. Phys. **145**, 307 (1990).

[11]A. Faulstich *et al.* (to be published).

[12]T. Sleator, O. Carnal, A. Faulstich, and J. Mlynek, Verh. Dtsch. Phys. Ges. (VI) **26**, 867 (1991).
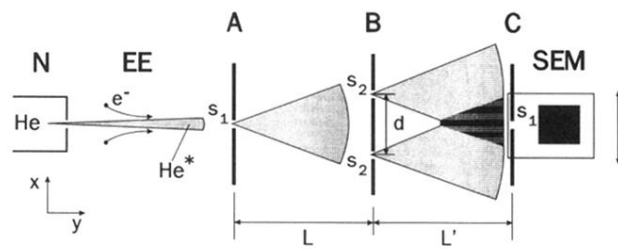
FIG. 2. Schematic representation of the experimental setup: nozzle system and gas reservoir N; electron impact excitation EE; entrance slit A, double slit B, and detector screen C; secondary electron multiplier SEM (mounted together with C on a translation stage). Dimensions: $d = 8$ μm, $L = L' = 64$ cm; slit widths: $s_1 = 2$ μm, $s_2 = 1$ μm.
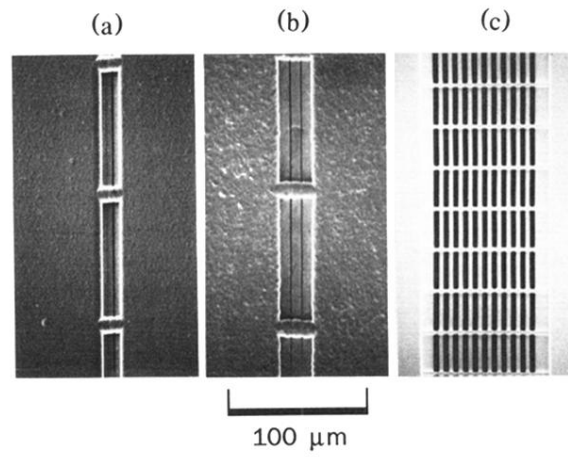
FIG. 3. Scanning-electron-microscope pictures of the microfabricated transmission structures, with the slit structures in the vertical direction and the support gratings in the horizontal direction: (a) entrance and detection slit (slit width $s_1 = 2$ μm); (b) double slit (slit width $s_2 = 1$ μm and slit separation $d = 8$ μm); (c) detection grating (grating periodicity 8 μm). The 100-μm scale is the same for all three pictures.